JOURNAL OF VIROLOGY, Mar. 2009, p. 2140–2153 Vol. 83, No. 5
0022-538X/09/$08.00+0 doi:10.1128/JVI.01871-08

Gene Regulation and Functional Alterations Induced by Kaposi's Sarcoma-Associated Herpesvirus-Encoded *ORFK13/vFLIP* in Endothelial Cells▽†

Shuhei Sakakibara,* Cynthia A. Pise-Masison, John N. Brady, and Giovanna Tosato

Laboratory of Cellular Oncology, Center for Cancer Research, National Cancer Institute, National Institutes of Health, Bethesda, Maryland 20892

Received 4 September 2008/Accepted 9 December 2008

Kaposi's sarcoma (KS) is an angioproliferative inflammatory disorder induced by endothelial cell infection with the KS-associated herpesvirus (KSHV). *ORFK13/vFLIP*, one of the KSHV genes expressed in KS, encodes a 188-amino-acid protein which binds to the Iκb kinase (IKK) complex to activate NF-κB. We examined *ORFK13/vFLIP* contribution to KS phenotype and potential for therapeutic targeting. Retroviral transduction of *ORFK13/vFLIP* into primary human endothelial cells induces the spindle morphology distinctive of KS cells and promotes the formation of abnormal vascular networks typical of KS vasculature; upregulates the expression of proinflammatory cytokines, chemokines, and interferon-responsive genes; and stimulates the adhesion of inflammatory cells characteristic of KS lesions. Thymidine phosphorylase, a cellular enzyme markedly induced by *ORFK13/vFLIP*, can metabolize the prodrug 5-fluoro-5-deoxyuridine (5-dFUrd) to 5-fluouridine (5-FU), a potent thymidine synthase inhibitor, which blocks DNA and RNA synthesis. When tested for cytotoxicity, 5-dFUrd (0.1 to 1 μM) selectively killed *ORFK13/vFLIP*-expressing endothelial cells while sparing control cells. These results demonstrate that *ORFK13/vFLIP* directly and indirectly contributes to the inflammatory and vascular phenotype of KS and identify 5-dFUrd as a potential new drug that targets KSHV latency for the treatment of KS and other KSHV-associated malignancies.

Kaposi's sarcoma-associated herpesvirus (KSHV/human herpesvirus 8) is the etiological agent of Kaposi's sarcoma (KS), primary effusion lymphoma (PEL), and a subset of multicentric Castleman's diseases. KS typically presents as a multicentric angioproliferative tumor characterized by multiple nodular or macular lesions often on the skin, and less frequently in the gastrointestinal tract and the lung. Histologically, the lesions consist of spindle cells infected with KSHV, inflammatory infiltrates of monocytes/macrophages, lymphocytes and other cells, and "vascular slits" replete of red blood cells (8). KS spindle cells are likely to be of endothelial lineage (19).

In KS tissues, KSHV establishes a mostly latent infection characterized by expression of a limited number of viral genes that are likely important to the disease pathogenesis (30). *ORFK13* is one such KSHV latent gene. Its gene product, called vFLIP (for viral Flice-like inhibitory protein) or K-FLIP, comprises two tandem death-effector domains that are often found in apoptotic signaling mediators such as cellular FLICE inhibitory protein (cFLIP) and caspase-8/FLICE. Consistent with its sequence similarity with cFLIP, vFLIP was found to inhibit caspase activation and prevent apoptotic cell death (39). Silencing *ORFK13/vFLIP* expression by RNA interference stopped PEL growth in vitro and in vivo, providing evidence of the essential role of K13/vFLIP in PEL pathogenesis (16). Transgenic mice of K13/vFLIP in lymphoid cells developed more lymphomas than controls (11). Similar to the viral proteins of many other lymphogenic viruses, K13/vFLIP activates NF-κB (1, 10, 25, 27, 42). By activating NF-κB and inhibiting the AP-1 pathway, K13/vFLIP was recently reported to promote viral latency (49).

Recent studies have characterized selected effects of K13/vFLIP expression in primary endothelial cells transduced with *ORFK13/vFLIP* (15, 20, 29), providing important insights into its function. Here, we broadly investigated K13/vFLIP function in endothelial cells. By establishing stable retrovirus-mediated transduction of *ORFK13/vFLIP* in primary human endothelial cells, we have extensively characterized the biochemical and functional consequences of K13/vFLIP expression in these cells.

MATERIALS AND METHODS

Cells. Human umbilical vein endothelial cells (HUVEC), isolated by collagenase digestion of umbilical veins, were cultured in HUVEC culture medium (M199 medium, 10% [vol/vol] fetal bovine serum [FBS]), human AB serum (5% [vol/vol]), heparin (25 μg/ml [Sigma-Aldrich, St. Louis, MO]), ascorbic acid (50 μg/ml [Sigma-Aldrich]), endothelial growth supplement from bovine neural tissue (15 μg/ml [Sigma-Aldrich]), L-glutamine (1.6 mM [Invitrogen, Carlsbad, CA]) and 1% (vol/vol) penicillin-streptomycin liquid (Invitrogen), as described previously (31). The human monocytic cell lines U937 and THP-1, the Burkitt's lymphoma cell line BL41, and the PEL cell line BCBL1 were cultured in RPMI 1640 GlutaMax-I medium (Invitrogen) with 10% heat-inactivated FBS. Phoenix, the retroviral packaging cell line (gifted from G. Nolan, Stanford University) was maintained in Dulbecco modified Eagle medium (high glucose)–GlutaMax-I medium (Invitrogen) with 10% FBS. Peripheral blood mononuclear cells were obtained from leukocyte-enriched peripheral blood (National Institute of Health, Clinical Center Blood Bank). Monocyte-enriched mononuclear cells

* Corresponding author. Mailing address: Laboratory of Cellular Oncology, Center for Cancer Research, National Cancer Institute, National Institutes of Health, 37 Convent Drive, Room 4134, Bethesda, MD 20892. Phone: (301) 594-9597. Fax: (301) 594-9585. E-mail: sakakibs@mail.nih.gov

† Supplemental material for this article may be found at http://jvi.asm.org/.

▽ Published ahead of print on 17 December 2008.

were obtained by positive selection with CD11b magnetic beads (Militenyi Biotec, Bergisch Gladbach, Germany).

Plasmids. The DNA fragment for the *K13* open reading frame was amplified from KSHV DNA (BC-1) by PCR with primers designing an amino-terminal FLAG epitope (DYKDDDDK) and inserted into the LZRSpBMN-IRES-GFP retroviral vector (G. Nolan) at the BamHI and EcoRI sites. A point mutation (A57L) was introduced in K13/vFLIP by conventional PCR techniques; nucleotide ^{169}GCG^{171}(Ala) in *ORFK13* was changed to ^{169}CTA^{171} (Leu). DNA sequencing confirmed accuracy of amplification and insertion (Applied Biosystems, Foster City, CA; DNA Sequencing Facility at National Cancer Institute, Bethesda, MD).

Retroviral infection. Plasmid transfection was performed with Lipofectamine 2000 (Invitrogen) as described by the manufacturer. Two days later, the supernatant was filtered (0.45-mm-pore-size filter) and Polybrene (hexadimethrine bromide [Sigma-Aldrich]) was added at a final concentration of 4 μg/ml. The viral supernatant was added to HUVEC (~80% confluence) grown on gelatin-coated 60-mm plastic plate, and the cells were spun (2,500 rpm, 30°C for 60 min). Immediately after the centrifugation, supernatant was replaced with fresh HUVEC culture medium, and cells were placed in incubator. Infection was evaluated based on green fluorescent protein (GFP) expression microscopically by Olympus IX51 (Olympus Optical, Melville NY) and/or by flow cytometry (FACSCalibur; BD Bioscience, San Diego, CA).

Matrigel cord formation assay. Cord formation on Matrigel was carried out as described previously (33). In brief, Matrigel (BD Bioscience, Bedford, MA) was solidified onto 48-well plates at 37°C for 30 min; 15,000 cells were seeded onto the gel. After 18 h of incubation, HUVEC formed a network of cord-like structure, observed by using bright-field microscopy. The number of angles was counted at low magnification (10× objective); five fields/well were counted, and the mean number of angles were averaged, as described previously (33).

Proliferation assay. HUVEC (1,500 cells/well) were cultured for 3 days in 96-well tissue culture plates (Corning Incorporated, Corning, NY) in M199 containing 18% FBS and 25 μg of heparin/ml with bFGF (25 ng/ml; R&D Systems, Minneapolis, MN), vascular endothelial growth factor (VEGF) (25 ng/ml; R&D Systems), or growth factor supplement from bovine neural tissue (15 μg/ml; Sigma Aldrich). Proliferation was measured by evaluating [methyl-^{3}H]thymidine uptake (0.6 μCi/well [0.022 MBq/well]; New England Nuclear, Beverly, MA) during the last 16 to 18 h of culture. Each assay was done in triplicate and repeated at least three times.

RNA preparation, microarray analysis, and RT-PCR. Total RNA was prepared with TRIzol (Invitrogen) according to the manufacturer's protocol. cRNA synthesis, hybridization with Affymetrix HG133A, and analyses were performed by the Virus Tumor Biology Section of Laboratory of Cellular Oncology, Center for Cancer Research, National Cancer Institute. For conventional reverse transcriptase PCR (RT-PCR), RNA was treated with DNase I (Invitrogen), and cDNA was synthesized by using avian myeloblastosis virus reverse transcriptase (Roche, Basel, Switzerland) with poly(dT) primer (Invitrogen) according to the manufacturer's protocol. One-twentieth of the reaction solution was used for PCR with *Taq* DNA polymerase (Invitrogen). Each reaction was loaded onto 1.5% agarose–TAE gel with ethidium bromide. For quantitative RT-PCR (qRT-PCR), cDNA was measured with SYBR green master mix kit (Applied Biosystems) by 7900HT fast real-time PCR system (Applied Biosystems). Each cycle threshold (C_T) was obtained from SDS2.3 software (Applied Biosystems) and normalized by the C_T of the housekeeping gene (*Gapdh* or β-*actin*). qRT-PCR experiments were performed in duplicate and repeated at least three times. The sequences of the primer sets were as follows: *Bcl2A1* (5′-CATTCTCAGCACA TTGCCTCAACAG-3′ and 5′-CCAGCCTCCGTTTTGCCTTATC-3′); *Cox2* (5′-GCATTCTTTGCCCAGCACTTC-3′ and 5′-CATCGCATACTCTGTTGT GTTCCC-3′); *Cxadr* (5′-AAAGCCAAAGGGGAAACTGC-3′ and 5′-GGCAC ATCTTCCCTGATATC-3′); *Emcn* (5′-CAAGCACTTCAGCAACCAGCC-3′ and 5′-TGTGAGAGAACAGGAGAGCCCC-3′); *Iap2* (5′-TGCCAAGTGGTT TCCAAGGTG-3′ and 5′-GTTGCTCTTTCTCTCTCCTCTTCCC-3′); *Icam1* (5′-TTGAACCCCACAGTCACCTATGG-3′ and 5′-TCCCTTCTGAGACCTC TGGCTTC-3′); *Il-6* (5′-GGAGAAGATTCCAAAGATGTAGCCG-3′ and 5′-T GGGTCAGGGGTGGTTATTGC-3′); *Ip-10* (5′-TGAAAGCAGTTAGCAAG GAAAGGTC-3′ and 5′-TGAAGCAGGGTCAGAACATCCAC-3′); *Isg15* (5′-ATGCTGGCGGGCAACGAATTCCAGGTG-3′ and 5′-GCCGCCTCCCCGC AGGCGCAGATTCAT-3′); *Mcp-2* (5′-GGAGAGATGGGTCAGGGATTC C-3′ and 5′-CAGACAGGTAGGAGGGAGAACAATG-3′); *Mip1A* (5′-CGGT GTCATCTTCCTAACCAAGC-3′ and 5′-CAGCCCTGAACAAAAGCATCC-3′); *Mx1* (5′-AAGATGGTTGTTTCCGAAGTGGAC-3′ and 5′-TCCTGGTAA CTGACCTTGCCTCTC-3′); *Lif* (5′-TCACCATCTGTGCCTTTGCTGC-3′ and 5′-CGGGGAAGAGAACGAAGAACCTAC-3′); *Lox-1* (5′-TGAAGGAC CAGCCTGATGAGAAGTC-3′ and 5′-TGAGCCCGAGGAAAATAGGTAA CAG-3′); *Pd-ecgf* (5′-TTCAATGTCATCCAGAGCCCAG-3′ and 5′-AGCCCC TCCACGAGTTTCTTAC-3′); *Rantes* (5′-CTCGCTGTCATCCTCATTGCTA C-3′ and 5′-CCTGGGGAAGGTTTTTGTAACTG-3′); *Sele* (5′-CCAGGTGA ACCCAACAATAGGC-3′ and 5′-GCACTCCATTCTCCAGAGGACATAC-3′); *Sema3C* (5′-TCAGCCTTTCCCACCATCCTTTAG-3′ and 5′-GCAGCGT CCTTTTCCAGATTCAC-3′); *Stat1* (5′-AGAACAGAGAACACGAGACCAA TGG-3′ and 5′-GCTGGAAAAGACTGAAGGTGCG-3′); *Vcam1* (5′-CACTT TATGTCAATGTTGCCCCC-3′ and 5′-TCCTGTCTCCGCTTTTTTCTTCA G-3′); *Xaf1* (5′-TTTTGATGTCAGAGCCCAAGCC-3′ and 5′-TCACCTTTCA CAAGACCACCACAG-3′); and *ORKF13* (5′-CCCTGTTAGCGGAATGTCT GTTTC-3′ and 5′-GTAAGAATGTCTGTGGTGTGCTGC-3′).

ELISA. Enzyme-linked immunosorbent assays (ELISAs) for IP-10, I-TAC, and MCP-2 were carried out by using ELISA kits from R&D Systems. Conditioned media were prepared in M199 medium with 1% FBS and 25 μg of heparin/ml from 3-day cultures of 80% confluent cells incubated in 12-well plates.

Indirect fluorescent staining. HUVEC infected with either control or K13/vFLIP-expressing retrovirus were seeded onto the fibronectin-coated four-chamber glass slides (BD Biosciences, San Jose, CA). Cells were washed with phosphate-buffered saline (PBS), fixed with 4% paraformaldehyde, and permeabilized with 1% Triton–PBS. Fixed cells were incubated with Alexa 546-conjugated phalloidin (Invitrogen) and DAPI (4′,6′-diamidino-2-phenylindole) for 10 min at room temperature. After a washing step, glass slides were mounted with Dako fluorescent mounting medium (Dako, Glostrup, Denmark).

AIDS-KS tissue specimens were fixed in paraformaldehyde and incubated in 15% sucrose in PBS overnight, followed by additional incubation in 30% sucrose in PBS for 1 to 2 days at 4°C. Tissue samples were embedded in OCT compound (Sakura Finetek, Tokyo, Japan), frozen in a dry ice-methyl butanol bath, and kept at −80°C. Frozen tissues were sliced, placed on glass slides, and stained with hematoxylin and eosin (Histoserv, Inc., Germantown, MD). For immunostaining, slides were fixed with 4% paraformaldehyde for 5 min at room temperature, washed in PBS, and then soaked in PBSTB (PBS plus 0.1% Triton, 1% bovine serum albumin, and 5% FBS) for 1 h at room temperature. Primary antibodies (1:200 dilution in PBSTB) were added to slides for 1 h at room temperature; slides were washed in PBS for 20 min, followed by additional incubation with secondary antibodies (1:500 dilution) for 1 h at room temperature. After being washed, the samples were mounted (mounting solution from Dako) and observed through a laser scanning confocal microscope LSM510 equipped with an objective lens (Plan Neofluar ×10/0.3; Carl Zeiss MicroImaging, Thornwood, NY). The pseudocolored images were converted into tiff files and exported into Adobe Photoshop (Adobe System, San Jose, CA).

Monocyte adhesion assay. THP-1, U937, and human CD11b$^+$ cells isolated from the peripheral blood were suspended in PBS at 10^7/ml with red fluorescent dye PKH26 (Sigma-Aldrich) for 10 min at room temperature. FBS was added to stop RKH26 uptake, and cells were washed with PBS. Labeled cells (30,000 cells/well) were added to HUVEC monolayers established in 48-well plate and incubated for 1 h. After washing to remove detached cells, adherent cells were counted under a fluorescence microscope Olympus IX51 phase-contrast microscope equipped with a ×4/0.13 PhC objective lens and a ×10 eyepiece (Olympus Optical, Melville, NY). The results reflect the counting of five replicate cultures/experiment.

Antibodies. For immunostaining: mouse anti-CD68 monoclonal antibody (clone Ki-M7; AbD Serotec, Raleigh, NC), goat anti-CD31 polyclonal antibody (BD Biosciences), and rabbit anti-VEGF antibody (Santa Cruz Biotechnology, Santa Cruz, CA). For Western blotting: mouse monoclonal anti-p65 antibody (BD Biosciences), goat anti-COX2 polyclonal antibody (Santa Cruz Biotechnology), rabbit anti-hIL-6 polyclonal antibody (Pepro Tech, Rocky Hill, NJ), goat anti-actin antibody (Santa Cruz Biotechnology), rabbit polyclonal antibodies to p38, phospho-p38 (Thr180/Tyr182), phospho-JNK (Thr183/Tyr185), phospho-AKT (Ser473), and anti-IkB mouse monoclonal antibody (Cell Signaling Technology, Danvers, MA).

Chemicals. Bay11-7082 {(E)3-[(4-methylphenyl)sulfonyl]-2-propenenitrile [Calbiochem, San Diego, CA]}, SB202190 [4-(4-fluorophenyl)-2-(4-hydroxyphenyl)-5-(4-pyridyl)-1H-imidazole], and 5-dFUrd were purchased from Sigma-Aldrich. KIN59 (5′-*O*-trityl-inosine) was kindly provided by J. Balzarini (Rega Institute for Medical Research, Leuven, Belgium) (24).

Cytotoxicity assay. On a gelatin-coated 96-well plate, either control or K13/vFLIP retrovirus-infected HUVEC was seeded (1,500 to 2,000 cells/well) and incubated for 2 h to allow cell attachment to the plate. Serial dilutions of 5-dFUrd in M199 complete HUVEC medium were added. In some experiments, the thymidine phosphorylase inhibitor, KIN59 (1 to 10 μM) or the same volume (0.1% [vol/vol]) of control dimethyl sulfoxide (DMSO) was added. Samples were tested in triplicate. After 48 h of culture, the cytotoxicity was evaluated by

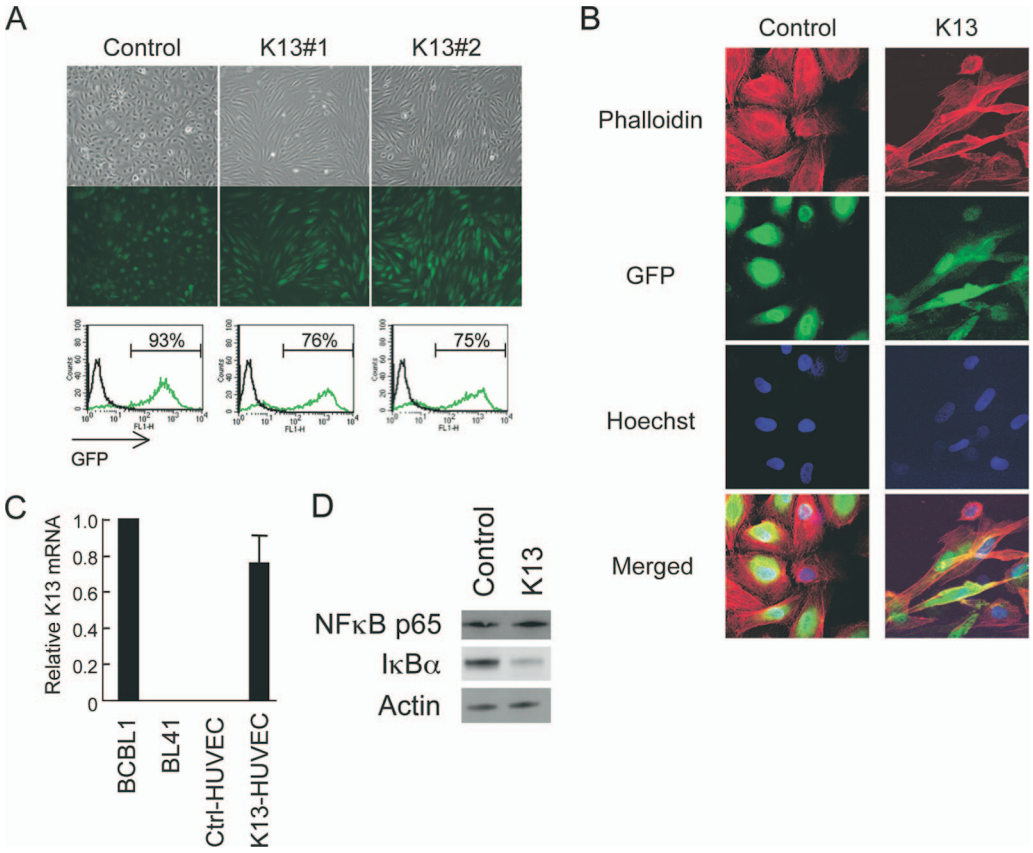

FIG. 1. Morphological changes in HUVEC transduced with K13/vFLIP retrovirus. (A) Two independent isolates of HUVEC were infected with *ORFK13/vFLIP-IRES-Gfp* retrovirus or *IRES-Gfp* retrovirus to yield K13#1 and K13#2 cultures. On day 3 after infection, living cells were observed under phase-contrast microscopy (original magnification, ×100, upper panels). Infectivity was evaluated by flow cytometric evaluation of GFP fluorescence (lower graphs). (B) Actin fibers stained by phalloidin in K13 (right)- and vector (left)-transduced cells growing on fibronectin-coated glass chamber slides observed by laser confocal microscopy (original magnification, ×63). (C) K13/vFLIP mRNA expression in BCBL1 cells and retrovirus-infected HUVEC measured by qRT-PCR. Burkitt's lymphoma BL41 cells were used as a negative control. (D) Western blot analysis of IκBα and NFκB p65 levels in cell lysates of K13/vFLIP- and control vector-infected HUVEC.

measuring the conversion rate of WST-8 [2-(2-methoxy-4-nitrophenyl)-3-(4-nitrophenyl)-5-(2,4-disulfophenyl)-2H-tetrazolium, monosodium salt] to WST-8 Formazan (Cell Counting Kit 8 [Dojindo Molecular Technologies, Gaithersburg, MD]) according to the manufacturer's protocol. The absorbance at 450 nm was measured by using a VersaMax turnable microplate reader (Molecular Devices, Sunnyvale, CA). The numbers of live cells were calculated from a standard curve generated with HUVEC. The results were then expressed as percentages of living cell numbers.

Statistical analysis. Results are expressed as means ± the standard deviation (SD). A Student *t* test was applied to evaluate group differences; a *P* value of <0.05 was considered significant.

RESULTS

Retroviral induction of KSHV *ORFK13/vFLIP*. We selected primary HUVEC for these studies because of their susceptibility to KSHV infection. HUVEC (from two separately derived populations; passage 2) were transduced with the *K13/vFLIP* gene by infection with a Moloney murine leukemia virus-derived retroviral vector carrying the *FlagORFK13-IRES-Gfp* gene cassette. As a control, we used HUVEC transduced with the empty retroviral vector. By day 3, more than 70% of control and K13-transduced HUVEC were GFP positive as measured by flow cytometry (Fig. 1A). At this time (day 3 after infection), *K13/vFLIP* retrovirus-infected HUVEC exhibited a dramatic change in shape to become elongated and resembling KS spindle cells (Fig. 1A and B). This change in cell morphology, not seen in control cells, persisted over subsequent propagation in culture over 3 weeks. When stained with fluorescent phalloidin, most K13/vFLIP-HUVEC displayed a prominent bipolar elongation of filamentous actin, which was not seen in control cells (Fig. 1B), a finding indicative of rearrangement of the actin cytoskeleton. By qRT-PCR, *K13/vFLIP* mRNA was specifically amplified from K13/vFLIP-HUVEC but not from control cells, and the level of *K13/vFLIP* expression was comparable to that found in BCBL-1 cells that are naturally infected with KSHV (Fig. 1C). Functional evidence for the presence of K13/vFLIP protein in K13/vFLIP-HUVEC was derived by analysis of IκBα, which is known to undergo ubiquitin-dependent degradation following K13/vFLIP binding to IKKγ and activation of IKK kinase activity (25). By Western blotting, we found that IκBα protein levels were markedly reduced in K13/vFLIP-HUVEC compared to control cells, whereas levels of the p65 subunit of NF-κB were unchanged (Fig. 1D).

Since K13/vFLIP activates the NF-κB pathway through its interaction with IKKγ and/or through TRAFs and NF-κB2/p100 (p52) (17, 28), and this pathway upregulates transcription

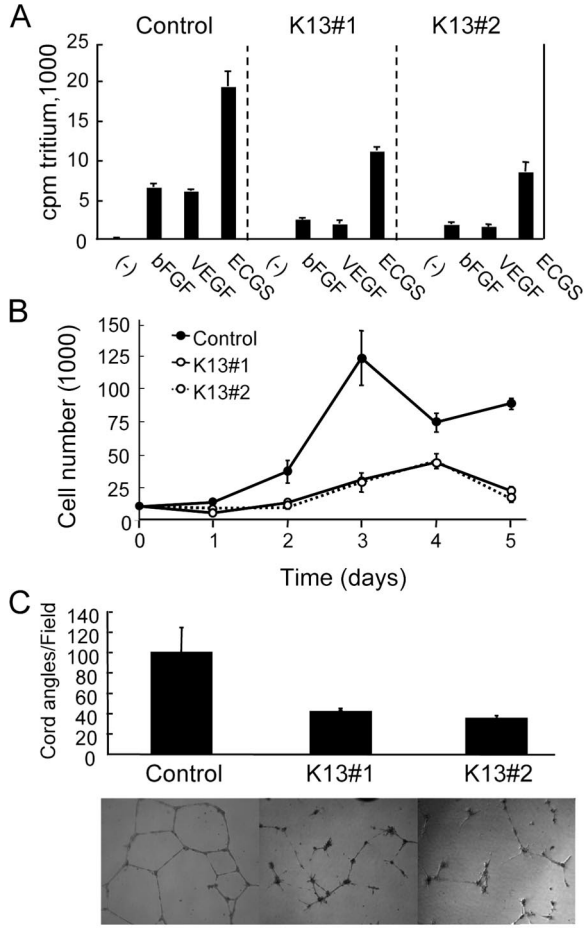

FIG. 2. Effects of K13/vFLIP transduction on HUVEC proliferation and ECM-dependent cord formation. (A) Proliferation assay. HUVEC transduced with either vector or K13/vFLIP-retrovirus were cultured (96-well plate) overnight without growth factors and then incubated for additional an 48 h in medium alone or medium supplemented with VEGF (25 ng/ml), bFGF (25 ng/ml), or endothelial cell growth supplement (ECGF [Sigma-Aldrich]). Proliferation was measured by [^{3}H]thymidine deoxyribose uptake during the last 16 h of culture. (B) Growth curve. Cells were seeded on gelatin-coated 48-well plates (10,000 cells/well). At each time point, cells were treated with trypsin and counted. Control and K13/vFLIP cells reached 100% confluence on days 4 and 5, respectively. (C) HUVEC (15,000 cells/well) were seeded onto 48-well plates coated with solidified Matrigel (BD Bioscience) and incubated at 37°C overnight. Cord angles were counted under phase-contrast microscopy (original magnification, ×40 [top graph]). Representative images of cord formation by control and K13-expressing HUVEC are shown (bottom panels). The results reflect the means (± SDs) of triplicate counts from three experiments.

of growth stimulatory and prosurvival genes, we tested the effect of K13/vFLIP expression on the growth and survival of HUVEC. Using tritium-labeled thymidine, we found that K13/vFLIP-HUVEC proliferated less vigorously than control cells in response to bFGF/FGF2, $VEGF_{165}$, and endothelial cell growth supplement (ECGF, a crude mixture of endothelial growth factor supplements from bovine neural tissue [Sigma-Aldrich]) (Fig. 2A). This reduced proliferation to ECGF by K13/vFLIP-HUVEC was associated with a reduction in the number of viable cells compared to control cells (Fig. 2B). K13/vFLIP-HUVEC did not undergo long-term outgrowth and did not display a prolongation in life span compared to control cells (not shown).

In additional analyses of the effects of K13/vFLIP in HUVEC function, we tested the extracellular matrix (ECM)-dependent formation of cordlike structures, an in vitro assay that recapitulates important steps of endothelial cell assembly into vascular structures, including cell attachment to the ECM, the generation of chemokine gradients, polarization, the formation of filopodia, cell migration, cell-to-cell attachment, and the formation of an orderly cord network (37). This is a tightly regulated, multistep morphogenic process, which involves dynamic change in the endothelial cells and is orchestrated by a variety of molecules. K13/vFLIP-HUVEC was consistently defective in its ability to form the characteristic network of cordlike structures produced by control cells. Microscopically, K13/vFLIP-HUVEC displayed reduced formation of cytoplasmic extensions connecting cells to each other and an increased tendency to form regularly distributed cell aggregates rather than connecting cords onto ECM (Fig. 2C). As a result, we documented a significant ($P < 0.01$) reduction in the number of intersecting angles formed by K13/vFLIP-HUVEC compared to control (Fig. 2C). Collectively, these results indicate that K13/vFLIP expression induces marked phenotypic and functional alterations in primary endothelial cells.

Analysis of gene expression regulated by K13/vFLIP. For a comprehensive analysis of changes in gene transcription induced by K13/vFLIP in HUVEC, Affymetrix GeneChip arrays were used. Two-independent experiments originated from different donor-derived HUVECs were carried out. After retroviral infection, each HUVEC was expanded under standard culture conditions for 7 to 10 days. Analysis of array results indicated that expression of a large number of genes was higher in K13/vFLIP-HUVEC than in control cells. Of 22,000 probe sets (14,500 genes), 499 probes detected a >2-fold increased expression (log ratio ≥ 1, signal strength > 150; see Table S1 in the supplemental material). The results for the most induced genes (log ratio ≥4) grouped by gene family are shown in Table 1.

The expression of chemokine genes known to stimulate chemotaxis in monocyte/macrophages and lymphocytes was markedly increased by K13/vFLIP, including *Ccl3*/*Mip1*A, *Ccl5*/*Rantes*, *Ccl20*/*Mip3*A, *Ccl8*/*Mcp-2*, *Cxcl2*/*Mip2*A, *Cxcl3*/*Mip2*B, *Cxcl5*/*Ena78*, *Cxcl6*/*Gcp-2*, *Cxcl10*/*Ip-10*, and *Cxcl11*/*I-tac*. Cytokine genes with proinflammatory and/or growth- stimulatory activities that were highly induced by K13/vFLIP included *Csf2*/*Gm-csf*, *IL-1A*, *IL-1B*, *IL-6*, *IL-11*, *IL-27b*/*Ebi3* (*EBV-inducible3*), and *Lif* (*leukemia inhibitory factor*). Of these gene products, secreted interleukin-1 (IL-1), IP-10, and I-TAC have been reported to variously affect endothelial cells (2, 36, 47). The IL-1 and IP-10 receptors are expressed in HUVEC (36, 47), and we found that CXCR7/RDC1, a receptor for I-TAC and SDF-1(9), is highly expressed in control HUVEC (data not shown) and is moderately (ca. 3.2- to 4.0-fold) augmented by K13/vFLIP (see Table S1 in the supplemental material).

Among genes found to be common targets of tumor necrosis factor alpha (TNF-α) stimulation (45, 46), *Traf1*, *Iap2*, and Tn*faip3*/*A20* were highly induced by K13/vFLIP in HUVEC, whereas TNF-α was not. These genes, together with *Tnip3* (Table 1), have been linked to initiation of a negative-feedback loop for NF-κB, occurring late in the course of inflammatory

TABLE 1. mRNAs strongly increased in K13/vFLIP-HUVEC compared to control HUVEC (log ratio ≥ 4)

Category and gene (abbreviation)	Probe set name	Gene accession no.	Ratio (log_2)[a] of K13/vFLIP to control cells in expt:	
			1	2
Chemokines				
CCL3/MIP1α	205114_s_at	NM_002983.1	9.3	6.5
CCL5/RANTES	1405_i_at	M21121	9.7	9.4
	204653_at	NM_002985.1	5.1	4.4
CCL20/MIP3α	205476_at	NM_004591.1	8.9	6.6
CCL8/MCP2	214038_at	AI984980	7.5	7.6
CXCL2/MIP2α	209774_x_at	M57731.1	5.0	3.0
CXCL3/MIP2β/GRO3	207850_at	NM_002090.1	6.6	5.4
CXCL5/ENA78	215101_s_at	BG166705	8.2	6.5
	214974_x_at	AK026546.1	8.0	5.8
CXCL6/GCP2	206336_at	NM_002993.1	6.0	5.6
CXCL10/IP10	204533_at	NM_001565.1	7.4	9.1
CXCL11/I-TAC	210163_at	AF030514.1	5.9	7.0
	211122_s_at	AF002985.1	6.1	6.7
CX3CL1/fractalkine	823_at	U84487	6.8	5.2
	203687_at	NM_002996.1	5.9	5.6
Cytokines, growth factors, and secreted ligands				
CSF2/GM-CSF	210229_s_at	M11734.1	8.2	5.5
CSF3/G-CSF	207442_at	NM_000759.1	7.3	4.9
IL-1α	210118_s_at	M15329.1	5.4	4.1
IL-1β	39402_at	M15330	7.7	4.4
	205067_at	NM_000576.1	6.7	4.5
IL-6	205207_at	NM_000600.1	5.3	5.8
IL-11	206924_at	NM_000641.1	5.4	3.2
IL-27b	219424_at	NM_005755.1	7.9	8.5
Leukemia inhibitory factor (LIF)	205266_at	NM_002309.2	5.3	4.1
Platelet-derived endothelial cell growth factor (PD-ECGF)	204858_s_at	NM_001953.2	2.9	5.8
SEMA3C/semaphorin E	203789_s_at	NM_006379.1	4.9	7.3
Complement component 3 (C3)	217767_at	NM_000064.1	4.6	4.3
Complement factor B (CFB)	202357_s_at	NM_001710.1	6.9	5.7
Complement C1s subcomponent (C1S)	208747_s_at	M18767.1	7.4	8.8
Receptors and other cell surface proteins				
Bone marrow stromal cell antigen 2 (BST2)	201641_at	NM_004335.2	4.6	4.5
HLA class II gamma chain	209619_at	K01144.1	3.2	5.2
Integrin α1	214660_at	X68742.1	3.9	4.4
Lectinlike ox-LDL receptor (LOX1)	210004_at	AF035776.1	6.9	9.5
TNF-α-induced protein 6 (TNFAIP6)	206025_s_at	AW188198	7.1	7.7
TNFR superfamily 9 (TNFRSF9/4-1BB)	207536_s_at	NM_001561.2	5.8	4.4
TNFR superfamily 11b (TNFSF11B/OPG)	204933_s_at	NM_002546.1	9.1	7.8
	204932_at	BF433902	7.1	8.3
VCAM1	203868_s_at	NM_001078.1	6.6	5.5
Apoptosis-related genes				
BCL2-related protein A1 (BCL2A1)/BFL1	205681_at	NM_004049.1	4.2	5.8
IAP2	210538_s_at	U37546.1	6.1	4.8
Superoxide dismutase 2 (SOD2)	215078_at	AL050388.1	3.6	4.7
	215223_s_at	W46388	4.6	3.6
TNFR-associated factor 1 (TRAF1)	205599_at	NM_005658.1	4.0	4.5
TNF-α-induced protein 3 (TNFAIP3)/A20	202644_s_at	NM_006290.1	4.1	4.8
	202643_s_at	AI738896	4.2	4.4
XIAP associated factor-1 (XAF1)	206026_s_at	NM_017523.1	8.7	7.5
	206133_at	NM_017523.1	4.1	5.1
Anti-virus and IFN-induced genes				
2′5′Oligoadenylate synthetase 1 (OAS1)	205552_s_at	NM_002534.1	3.9	5.6
	202869_at	NM_016816.1	3.6	5.6
	204972_at	NM_016817.1	5.5	7.0
2′5′Oligoadenylate synthetase 1 (OAS2)	206553_at	NM_002535.1	4.7	4.2
2′5′Oligoadenylate synthetase 3 (OAS3)	218400_at	NM_006187.1	3.6	4.6
2′5′Oligoadenylate synthetase-like (OASL)	210797_s_at	AF063612.1	4.0	5.4

Continued on following page

TABLE 1—*Continued*

Category and gene (abbreviation)	Probe set name	Gene accession no.	Ratio (log_2)[a] of K13/vFLIP to control cells in expt:	
			1	2
	205660_at	NM_003733.1	3.1	5.2
APOBEC3G	204205_at	NM_021822.1	3.8	4.7
Diubiquitin (UBD)	205890_s_at	NM_006398.1	11.8	8.4
Hect domain and RLD 6 (HERC6)	219352_at	NM_017912.1	4.3	5.5
Interferon alpha-inducible protein 6 (IFI6)	204415_at	NM_022873.1	5.8	6.1
Interferon gamma-inducible protein 30 (IFI30)	201422_at	NM_006332.1	4.8	5.0
Interferon-induced protein (IFI44)	214453_s_at	NM_006417.1	3.6	5.3
	214059_at	BE049439	3.8	4.7
Interferon-induced protein 35 (IFI35)	209417_s_at	BC001356.1	4.1	5.8
Interferon-induced protein with TRP 1 (IFIT1)	203153_at	NM_001548.1	9.3	12.1
Interferon-induced protein with TRP 4 (IFIT4)	204747_at	NM_001549.1	4.6	6.4
Interferon-induced transmembrane protein 2 (IFITM2)	201601_x_at	NM_003641.1	4.8	4.7
	214022_s_at	AA749101	4.5	5.0
Interferon-inducible protein 44-like	204439_at	NM_006820.1	6.8	8.4
Interferon-stimulated gene, 15 kDa (ISG15)	205483_s_at	NM_005101.1	4.9	3.8
Interferon-stimulated gene, 20 kDa (ISG20)	204655_at	NM_002985.1	5.6	8.1
	204698_at	NM_002201.2	5.1	5.2
	33304_at	U88964	4.3	4.2
Melanoma differentiation-associated protein 5 (MDA5)	219209_at	NM_022168.1	4.4	4.7
Myxovirus resistance 1 (MX1)	202086_at	NM_002462.1	6.1	7.0
Myxovirus resistance 2 (MX2)	204994_at	NM_002463.1	6.7	8.0
Retinoic acid- and interferon-inducible protein, 58 kDa	203595_s_at	N47725	3.3	5.7
	203596_s_at	NM_012420.1	3.2	4.9
Viperin/cig5	213797_at	AI337069	6.2	9.5
Transcription				
ATF-like 3 (B-ATF3)	220358_at	NM_018664.1	4.8	3.9
C/EBP delta	203973_s_at	NM_005195.1	4.6	4.2
NKX3.1	209706_at	AF247704.1	5.0	4.9
mSin3B	222095_s_at	AW450345	5.7	6.6
Similar to mSin3B	209353_s_at	BC001205.1	5.6	4.4
Others				
Carbonic anhydrase VIII (CA8)	220234_at	NM_004056.2	4.2	4.7
Caspase-1 (CASP1)	211368_s_at	U13700.1	3.5	4.6
Galectin 3-binding protein (LGALS3BP)	200923_at	NM_005567.2	4.9	5.4
Kynureninase (L-kynurenine hydrolase)	210663_s_at	BC000879.1	7.0	8.6
	217388_s_at	D55639.1	7.1	8.3
	204385_at	NM_003937.1	5.2	5.6
Laminin γ2 (LAMC2)	202267_at	NM_005562.1	6.6	5.8
	207517_at	NM_018891.1	6.8	4.1
MMP7	204259_at	NM_002423.2	2.4	6.3
Plasminogen activator inhibitor 2 (PAI2)	204614_at	NM_002575.1	5.6	5.2
Pregnancy-associated plasma protein A (PAPPA)	201981_at	AA148534	5.4	5.8
Proteasome subunit beta 9 (PSMB9)	204279_at	NM_002800.1	5.0	6.6
Receptor transporter protein 4 (RTP4)	219684_at	NM_022147.1	5.1	6.2
Similar to differential display and activated by p53 (DDA3)	201645_at	BC001425.1	7.4	5.2
Solute carrier family 15 A3 (SLC15A3)	219593_at	NM_016582.1	5.4	7.4
TNFAIP3 interacting protein 3 (TNIP3)	220655_at	NM_024873.1	4.5	4.4

[a] The results are expressed as ratios of K13/control (log_2) in two experiments.

responses (21, 48). A number of IFN-inducible genes were also highly induced in K13/vFLIP-expressing HUVEC. A previous study (45) found that endothelial cells treated with TNF-α display increased expression of the IFN-inducible genes *2′5′ oligoadenylate synthetase 1* (*Oas1*), *diubiquitin* (*Ubd*), *interferon-induced protein 44* (*Ifi44*), *interferon-stimulated gene 20 kD* (*Isg20*), *melanoma differential associated protein 5* (*Mda5*), and *myxovirus resistance 1* (*Mx1*). We found these same genes to be

TABLE 2. mRNAs decreased in K13-expressing HUVEC compared to control HUVEC (log ratio ≥ 2)

Gene (abbreviation)	Probe set name	Gene accession no.	Ratio (log_2)[a] of K13/control in expt:	
			1	2
BMP 4	211518_s_at	D30751.1	–2.1	–5.2
Clusterin	222043_at	AI982754	–1.8	–3.8
	208791_at	M25915.1	–1.9	–3.1
	208792_s_at	M25915.1	–1.7	–3.3
Coxsackievirus and adenovirus receptor (CXADR)	203917_at	NM_001338.1	–1.6	–5.5
Endomucin	219436_s_at	NM_016242.1	–2.4	–4.6
Furry homolog (FRY)	214319_at	W58342	–1.7	–3.4
G protein-coupled receptor 126	213094_at	AL033377	–1.8	–4.0
IMAGE135460	214920_at	R33964	–1.2	–4.1
Integrin alpha 6	215177_s_at	AV733308	–1.8	–3.3
	201656_at	NM_000210.1	–1.7	–3.4
LIM domain binding 2 (LDB2)	206481_s_at	NM_001290.1	–1.3	–3.8
Matrix Gla protein (MGP)	202291_s_at	NM_000900.1	–2.0	–2.9
Multimerin (MMRN)	205612_at	NM_007351.1	–1.9	–3.2
Paraneoplastic antigen 2 (PNMA2)	209598_at	AB020690.1	–2.3	–3.2

[a] The results are expressed as ratios of K13 to control in two experiments.

induced by K13/vFLIP expression in HUVEC. Other IFN-inducible genes that we found induced by K13/vFLIP in HUVEC include *Apobec3G*, *Isg15*, [scapi]l-*kynurenine hydrolase* (*Kynu*) (18), and *receptor* (*chemosensory*) *transporter protein 4* (*Rtp4*) (14).

In contrast to its activity as a broad inducer of transcription, K13/vFLIP substantially diminished the expression of only few genes in HUVEC (Table 2 and see Table S2 in the supplemental material), including *Coxackievirus and adenovirus receptor* (*Cxadr*) and *G-protein-coupled receptor 126* (*Gpr126*), whose repression was previously noted in TNF-α-treated endothelial cells (45).

We performed RT-PCR, ELISA, and immunoblotting to confirm selected microarray results. By conventional RT-PCR, we confirmed increased expression of a number of genes (Fig. 3A). Although *Isg15*, *IL-6*, *Stat1*, *Iap2*, and *Bcl2A* were detected in the control cells, most of the other mRNAs were only detected in the K13/vFLIP-HUVEC in conventional RT-PCR, suggesting that expression of these genes was switched on by a K13/vFLIP-mediated pathway. By qRT-PCR (Fig. 3B), we documented a 10- to 40-fold increase in the expression of the *Stat1*, *Icam1*, *Pd-ecgf*, *Cox2*, and *Isg15* genes in K13/vFLIP-HUVEC (day 10 after transduction) compared to controls. We also found that *Ip-10* mRNA was strongly induced (as much as 2,000-fold) and that *Cxadr* and *Emcn* mRNAs were reduced (by ~90%) in HUVEC by K13/vFLIP. By ELISA (Fig. 3, C), we detected increased levels of IP-10 (~20-fold increase), I-TAC (~8-fold increase), and MCP-2 (not detectable in the control conditional medium) in the culture supernatant of K13/vFLIP-HUVEC compared to the control. It is worth noting that K13/vFLIP-HUVEC culture supernatants contained IP-10 at sufficiently high levels (16.5 ± 1.3 ng/ml) to negatively regulate endothelial cell growth and ECM-dependent cord formation (2). By Western blotting (Fig. 3D), we confirmed increased expression of IL-6 and COX2 (cycloexogenase2) in K13/vFLIP-HUVEC compared to the control.

Involvement of the NF-κB pathway in the regulation of gene expression by K13/vFLIP. To examine whether K13/vFLIP modulates gene expression through the NF-κB pathway, we used Bay11-7082, an inhibitor of NF-κB activity (35). On day 5 after retrovirus infection, 5 μM Bay11-7085 or vehicle (dimethyl sulfate [DMSO]) was added to K13/vFLIP-transduced HUVEC, and on day 7 the cells were harvested (Fig.4Aa). At the time of harvest, the spindle cell morphology induced by K13/vFLIP was slightly reversed by Bay11-7085, but the drug-containing cell cultures were sparse (Fig.4Ab), suggesting drug toxicity. By qRT-PCR, Bay11-7085 reduced by at least 50% expression of *Icam1*, *Vcam1*, *Cox2*, and *Ip-10*, which was upregulated in K13/vFLIP-HUVEC treated with DMSO compared to control HUVEC (Fig.4Ac). These results suggested a role for the NF-κB pathway in gene regulation by K13/vFLIP, but the presence of drug toxicity that may differently affect the stability of distinct mRNAs prompted additional experiments.

Bagneris et al. reported the crystal structure of the K13/vFLIP-IKKγ complex, revealing that the molecular cleft on the death-effector domain of K13/vFLIP represents a binding platform for IKKγ helices (amino acids 150 to 270) (4). Ala57 located in one of two clefts of K13/vFLIP was found to be critical for IKKγ binding because A57L substitution caused K13/vFLIP to both lose physical interaction with IKKγ in vitro and the ability to activate NF-κB in a transient reporter assay (4). To overcome the limitations of the experiments with Bay11-7082, we engineered an A57L mutation into the retroviral expression vector for K13/vFLIP. Unlike wild-type K13/vFLIP, mutant K13/vFLIP^{A57L} transduced into HUVEC did not change the cell morphology (Fig.4Ba). This difference could not be attributed to reduced HUVEC infection by the mutant K13/vFLIP^{A57L}, as assessed by microscopic evaluation of GFP expression. On day 5 after infection, cells were harvested for RNA extraction. Compared to wild-type K13/vFLIP, which clearly induced expression of the *Icam1*, *Stat1*, *Cox2*, *Vcam1*, and *Ip-10* genes (albeit to a somewhat lower degree than that observed in cells on day 7 or 10 after infection), the mutant K13/vFLIP^{A57L} failed to induce the expression of the *Icam1*, *Stat1*, *Cox2*, and *Vcam1* genes and stimulated very little *Ip-10* expression (Fig.4Bb). *Emcn* expression, which is suppressed by K13/vFLIP transduction, showed no reduction by K13/vFLIP^{A57L}. Thus, we conclude that the K13/vFLIP-IKKγ

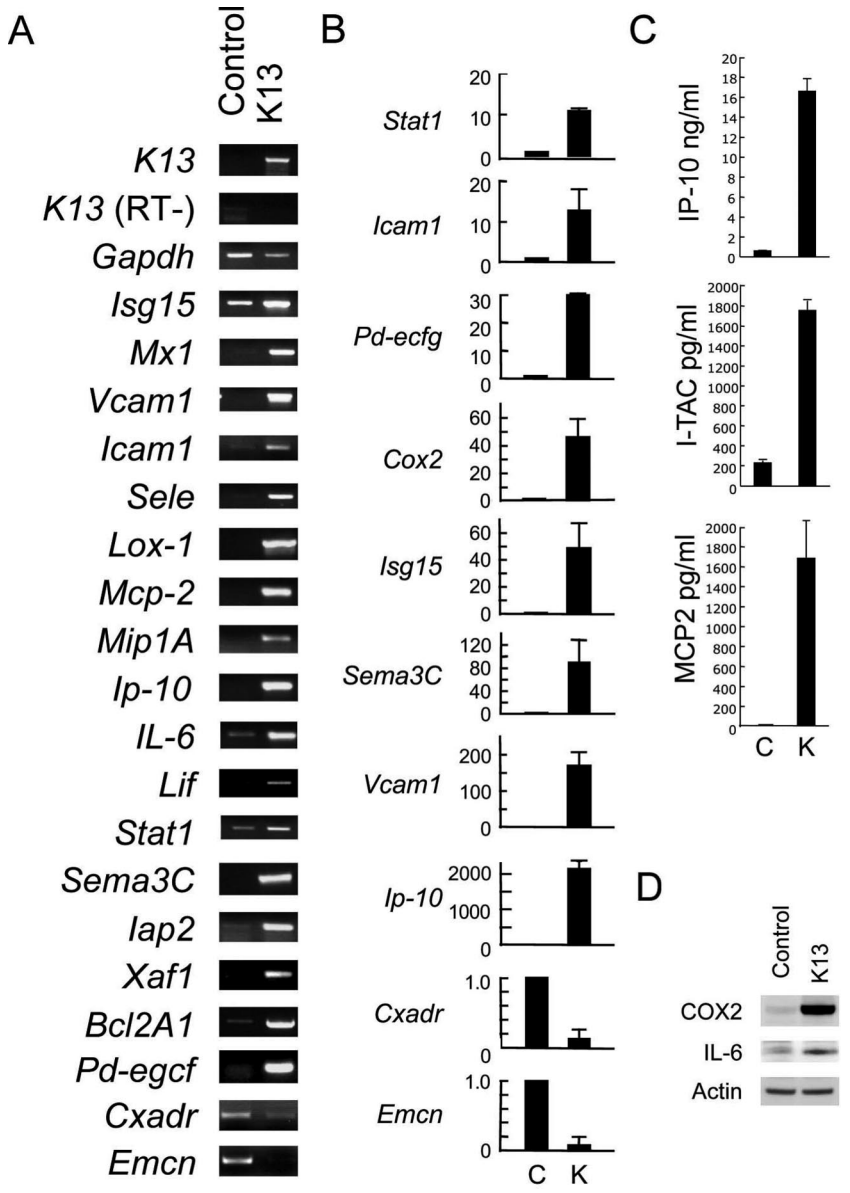

FIG. 3. Gene regulation by K13/vFLIP in HUVEC. (A) RT-PCR for selected genes. Amplified DNAs were loaded onto 1.5% agarose–TAE gels and visualized by ethidium bromide. (B) Fold change in expression levels of selected genes evaluated by qRT-PCR. Expression levels were normalized by *Gapdh* and expressed as the fold change compared to control. (C) Secretion of IP-10, I-TAC, and MCP-2 evaluated by ELISA. Each supernatant was harvested from 3-day cultures of K13/vFLIP-expressing or control HUVEC in 12-well plates. The results reflect the mean concentrations (± the SD) from two or three independent experiments. (D) Western blotting for COX2, IL-6, and actin. Equal amounts of cell lysates were immunoblotted with specific antibodies.

axis is critical to K13/vFLIP modulation of gene expression in HUVEC. Other studies will be required to establish whether K13/vFLIP can recruit additional pathways for regulation of selected genes.

SAPK activation in K13/vFLIP-expressing HUVEC. The pattern of gene and protein expression in K13/vFLIP-HUVEC resembled, at least in part, the pattern induced in HUVEC by inflammatory-type cytokines. We found the expression of two such cytokines, IL-1α and IL-1β to be highly induced by K13/vFLIP in HUVEC (Table 1), which express the cognate surface receptors for these cytokines. Since IL-1α and IL-1β, and other inflammatory cytokines are known to induce activation of the mitogen-activated protein kinases (MAPKs) p38/SAPK2 and JNK/SAPK (12), we examined their phosphorylation status in K13/vFLIP-HUVEC. As shown in Fig. 4A, JNK/SAPK was markedly more phosphorylated in K13-HUVEC compared to the control, and p38 was slightly more phosphorylated in K13-HUVEC compared to controls. STAT1 (for signal transducer and activator of transcription 1) is a transcription factor activated by a variety of signals, including signals from a TNF-induced autocrine loop mediated by interferon regulatory factors (IRF1/3) (49). Interestingly, phosphorylated STAT1 (tyrosine-701) was also markedly increased in K13/vFLIP-HUVEC compared to control (Fig. 5A). It may be related to

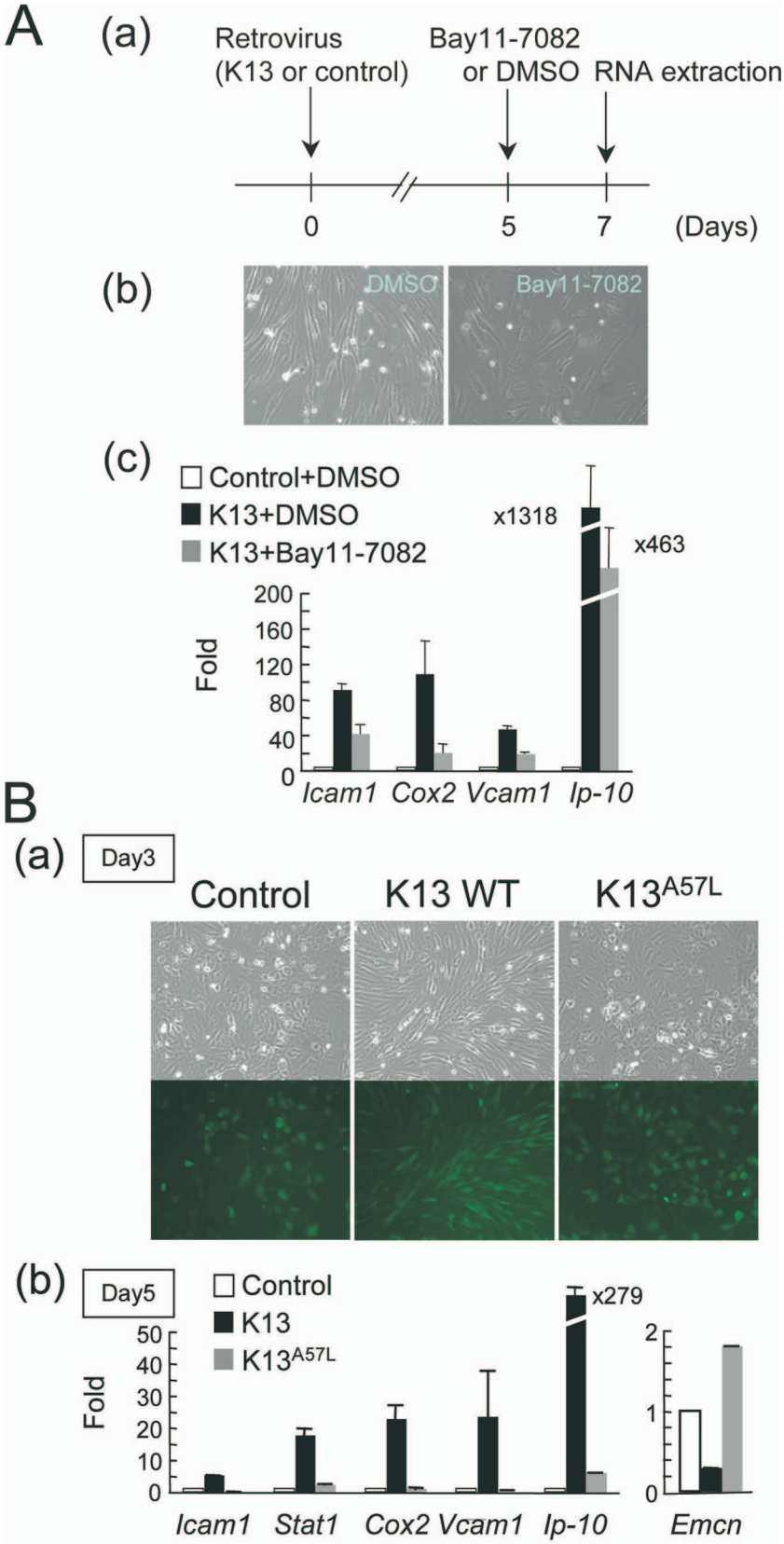

FIG. 4. The IKK/IκB/NF-κB pathway is critical for altered gene expression by K13/vFLIP. (A) Effects of the NF-κB inhibitor Bay11-7082. (a) Schematic representation of the experiment. (b) Representative microscopic morphology of K13/vFLIP-HUVEC treated with DMSO or Bay11-7082 for 2 days (original magnification, ×200). (c) qRT-PCR for *Icam1*, *Cox2*, *Vcam1*, and *Ip-10* in K13/vFLIP-HUVEC treated with DMSO or

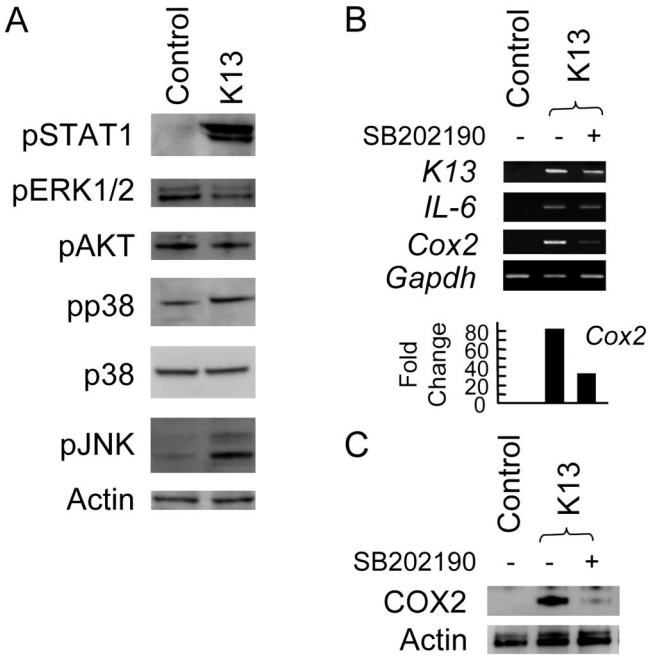

FIG. 5. Activation of STAT1, JNK, and p38 in K13/vFLIP-expressing HUVEC; p38 activation is required for COX2 expression. (A) Western blot analysis of cell lysates from HUVEC infected with K13/vFLIP or control retrovirus. (B) RT-PCR analysis of *Gapdh*, *Il-6*, *Cox2*, and *K13/vFLIP* expression in untreated HUVEC and HUVEC treated with SB202190. The bar graph depicts the relative expression of *Cox2* measured by qRT-PCR (normalized by *Gapdh*). (C) Western blot analysis of COX2 levels in HUVEC after 2-day incubation with or without 10 μM SB202190.

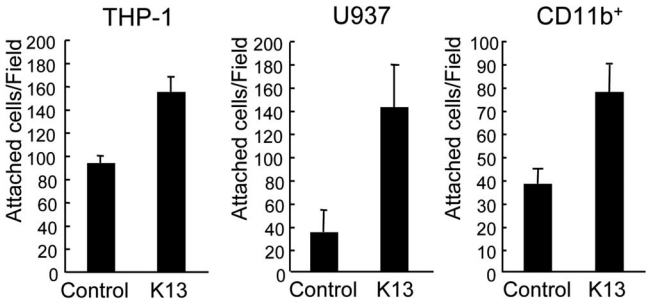

FIG. 6. Enhanced monocyte attachment to HUVEC induced by K13/vFLIP. Red fluorescence-labeled THP1 cells, U937, and purified peripheral CD11b$^+$ cells were incubated onto monolayers of HUVEC transduced with K13/vFLIP or empty retrovirus. After 2 h of incubation, the wells were washed twice with PBS, and attached cells were counted under fluorescence microscopy. Each sample was counted five times, and the average numbers (± the SD) are shown. Representative results from three experiments are shown.

increased *Stat1* expression (Fig. 3A and B) or be the result of activation by signals indirectly induced by K13/vFLIP expression. Phosphorylated STAT3 was not detected (not shown), and the kinases ERK1/2 and AKT (Ser473) displayed similar degrees of phosphorylation in K13/vFLIP and control HUVEC (Fig. 5A).

Previously, TNF-α-induced *Cox2* expression in endothelial cells was reported to be p38 MAPK/SAPK dependent (44). We now tested whether the p38 MAPK/SAPK pathway is involved in K13-induced activation of *Cox2* in HUVEC. The p38 MAPK/SAPK inhibitor SB202190 (10 μM), selectively reduced *Cox2* expression in K13/vFLIP-HUVEC as detected by RT-PCR (Fig. 5B) and Western blotting (Fig. 5C). In contrast, expression of K13/vFLIP and expression of *IL-6*, which was markedly induced by K13/vFLIP in HUVEC (Fig. 3C and Table 1), was not significantly altered by the p38 MAPK/SAPK inhibitor (Fig. 5B). These results provide evidence that the p38 MAPK/SAPK pathway is required for COX2 stimulation in K13/vFLIP-HUVEC.

Monocyte/macrophage attachment to K13/vFLIP-expressing HUVEC, infiltration of KS tissue, and VEGF expression. K13/vFLIP induced an "inflammatory-type" phenotype in HUVEC by promoting the secretion of inflammatory-type cytokines/chemokines and stimulating expression of *Icam1* and *Vcam1* (Table 1). Since inflammatory capillary endothelium is known to promote the recruitment of inflammatory leukocytes to sites of inflammation (22), we examined leukocyte attachment to K13/vFLIP-HUVEC. CD11b$^+$ mononuclear cells purified from peripheral blood and monocytic lineage THP-1 and U937 cell lines were fluorescein labeled and incubated (1 h, 37°C) on monolayers of either control or K13/vFLIP-expressing HUVEC. After removal of the nonadherent cells, cell attachment was measured. As shown in Fig. 6, we found that all cells tested displayed a significantly ($P < 0.01$) greater attachment to K13/vFLIP-HUVEC compared to control HUVEC. This indicates that K13/vFLIP expression in endothelial cells promotes monocyte/macrophage adhesion to these cells.

Monocyte/macrophages often infiltrate KS tissues (8), an observation confirmed here by CD68 immunostaining of a representative KS tissue from an untreated patient (Fig. 7). KS tissues are rich in VEGF (38), an observation confirmed here by VEGF immunostaining (Fig. 7B). Since K13/vFLIP did not promote VEGF mRNA expression in HUVEC (Table 1 and see Fig. S1 in the supplemental material), and VEGF was not detectable by ELISA in the culture supernatants of K13/vFLIP-HUVEC (not shown), we examined the possibility that K13/vFLIP might indirectly contribute to VEGF expression in KS tissues. Double staining for monocyte/macrophages (CD68, red) and VEGF (green) showed colocalization (yellow) in a proportion of cells (Fig. 7C), demonstrating that inflammatory cells of monocyte/macrophage lineage are a source for VEGF

Bay11-7082 for 2 days; the results are shown as the fold change compared to control HUVEC treated with DMSO (0.1% [vol/vol]). (B) Loss-of-function mutation at A57 in K13/vFLIP affected on morphological and transcription changes. (a) Representative microscopic morphology of HUVEC transduced with control, wild-type K13/vFLIP and its mutant A57L retrovirus 3 days after infection (original magnification, ×100). (b) qRT-PCR for *ICAM1*, *Stat1*, *Cox2*, *Vcam1*, *Ip-10*, and *Emcn* in HUVEC transduced with control, wild-type K13/vFLIP and its mutant A57L retrovirus 3 days after infection. The results are shown as the fold change compared to control HUVEC.

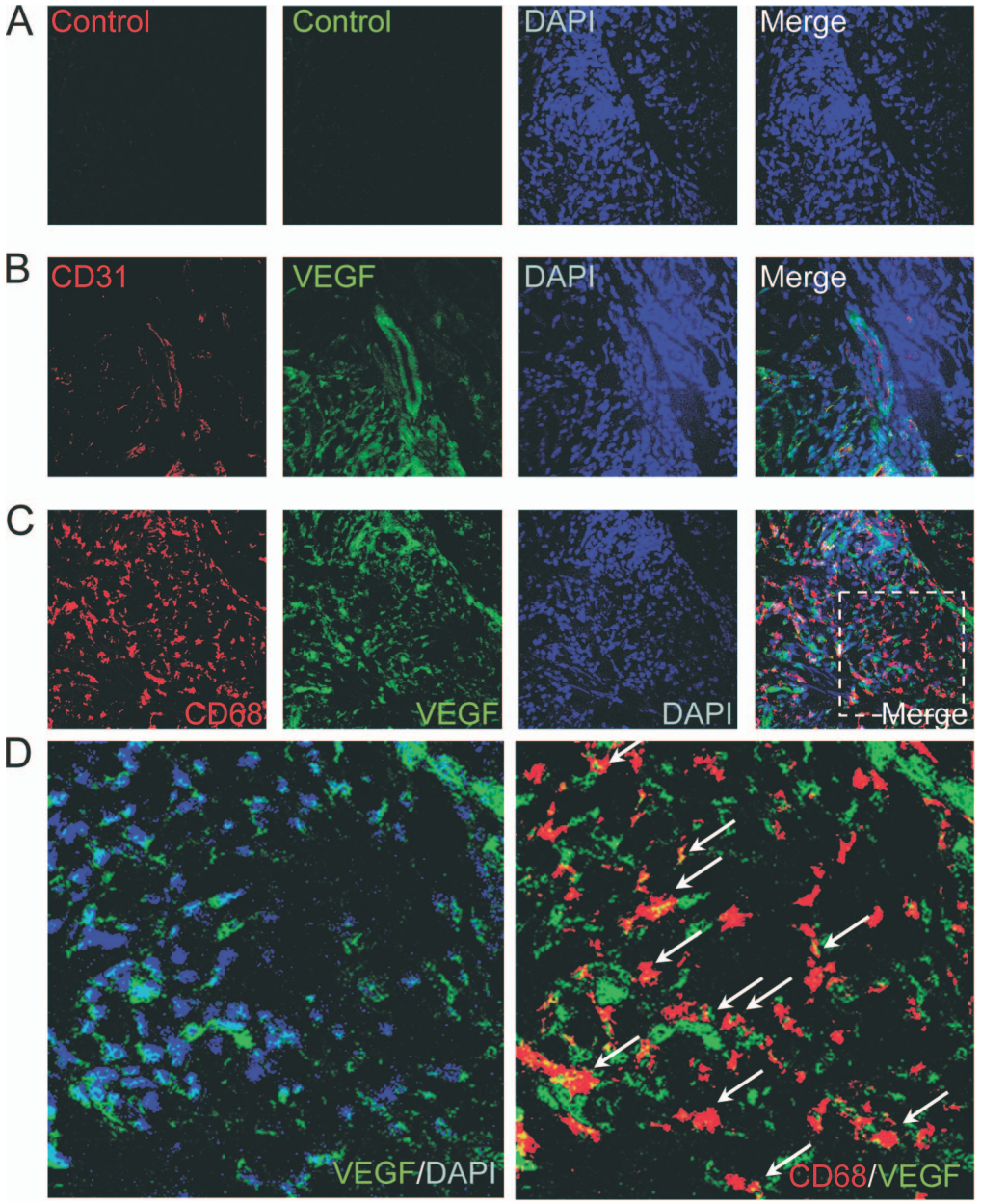

FIG. 7. CD68$^+$ monocyte/macrophages infiltrate KS tissue. Frozen sections of KS biopsy tissue on glass slides were observed by laser confocal microscopy. Control antibodies (mouse, rabbit, and goat immunoglobulins) were stained with DAPI (A), goat anti-human CD31 antibody plus rabbit anti-VEGF antibody (B), and mouse anti-human CD68 monoclonal antibody plus rabbit anti-VEGF antibody (C). As secondary antibodies, Alexa 488-conjugated anti-rabbit, Alexa 546-cojugated anti-mouse, and Alexa 546-cojugated anti-goat antibodies were used. DNA was stained by using DAPI. (D) Enlargement of the area outlined by the dotted white line in panel C. Arrows point to the cells expressing both CD68 and VEGF (yellow, right panel).

in KS lesions. Additional cells besides CD68$^+$ cells expressed VEGF, including some vascular mural cells surrounding CD31$^+$ cells (Fig. 7B). These observations provide evidence that KSHV through K13/vFLIP contributes to the recruitment of inflammatory cells and to VEGF accumulation in KS tissues.

Enhanced biological activity of 5-dFUrd induced by K13/vFLIP. *ORFK13* transduction in HUVEC greatly stimulated the expression of *Pd-Ecgf* (for platelet-derived endothelial cell growth factor) (Table 1 and Fig. 3A). PD-ECGF is also a thymidine phosphorylase (TP) (34), which can catalyze the conversion of thymidine + phosphate into thymine + 2-deoxy-D-ribose-1-phosphate (7). A substrate for TP is 5-dFUrd, a pyrimidine nucleoside with antineoplastic activity, which is largely dependent upon its enzymatic conversion to 5-FU by PD-ECGF/TP (3, 6) (Fig. 8A). Increased expression of PD-ECGF/TP in K13/vFLIP-HUVEC would be expected to cause an increased conversion of 5-dFUrd prodrug into 5-FU. We compared the cytotoxic effects of 5-dFUrd on K13/vFLIP-HUVEC and control HUVEC. After 48 h of incubation with

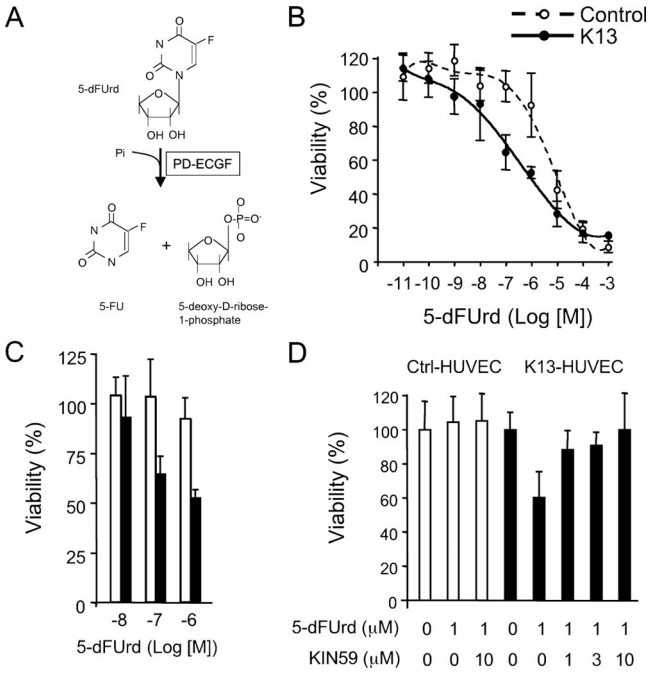

FIG. 8. Concentration-dependent cytotoxicity of 5-dFUrd for K13/vFLIP-transduced and control HUVEC. (A) Chemical structure of 5-dFUrd and its metabolite 5-FU. PD-ECGF/TP converts 5-dFUrd into 5-F (P_i = inorganic phosphate). (B) Viability of HUVEC infected with either control or K13-coding retrovirus after 48-hour incubation with 5-dFUrd-containing medium. Cell viability was measured by using a Cell Counting Kit-8 (Dojindo). The results reflect the percent viability (± the SD). Representative results of three experiments performed are shown. (C) HUVEC viability after 48 h of incubation with 0.01, 0.1, and 1 μM 5-dFUrd. The results are expressed as the percent viability in medium only and reflect the means (± the SD) of three experiments. (D) KIN59 reverses 5-dFUrd-induced cytotoxicity for K13/vFLIP-HUVEC. Control and K13/vFLIP-HUVEC were treated with 5-dFUrf (1 μM) with or without KIN59 (1, 3, or 10 μM) for 48 h. The results reflect % viability in medium only and represent the means (± the SD) of three experiments.

5-dFUrd at concentrations ranging between 0.01 nM and 1 mM, we found that K13-expressing HUVEC were significantly more sensitive than control to 5-dFUrd (Fig. 8B): 50% of the K13-HUVEC (black dots) were killed at a drug concentration as low as 1 μM, a drug concentration that minimally affected the viability of control cells (open dots in Fig. 8B). A 5-dFUrd concentration of 10 μM was required to kill ~60% of the control cells, and a drug concentration of 100 μM killed most control and K13/vFLIP-HUVEC (Fig. 8B). We determined that the 50% effective dose for 5-dFUrd is 13 μM for control HUVEC and 1.1 μM for K13/vFLIP-HUVEC, an ~10-fold difference. These experiments demonstrate that K13/vFLIP-HUVEC is significantly more sensitive to 5-dFUrd than control cells.

Finally, to address whether PD-ECGF/TP contributed to the increased 5-dFUrd susceptibility of K13/vFLIP-HUVEC, we used a chemical inhibitor of PD-ECGF/TP, KIN59 (5′-*O*-trityl-inosine) (24). KIN59 inhibits the conversion of thymidine to thymine by *E. coli* TP and human PD-ECGF/TP in vitro and in vivo as determined by the chick chorioallantoic membrane assay (23). Because we found that 80 μM KIN59 killed 50% of HUVEC (data not shown), we tested KIN59 at concentrations ranging between 1 μM and 10 μM. As shown in Fig. 8D, the cytotoxicity of 5-dFUrd for K13/vFLIP-HUVEC was significantly reduced by KIN59 (black bars), which displayed no effects on the viability of control cells (white bars). These results indicate that the increased *Pd-ecgf* expression in K13/vFLIP-HUVEC is responsible for the augmented cytotoxicity of 5-dFUrd.

DISCUSSION

We show that expression of the KSHV *ORFK13/vFLIP* gene in endothelial cells contributes to the proinflammatory phenotype, the spindle cell morphology, and the characteristic vascular lesions of KS. We find that K13/vFLIP does not directly promote expression of genes linked to increased cells growth while inducing selected antiapoptotic proteins such as *Iap2* and Bcl2-related A1 (Table 1). However, by indirectly stimulating the expression of VEGF and other growth factors, K13/vFLIP may ultimately contribute to the proliferative phenotype of KS lesions.

The proteins IL-6, granulocyte-macrophage colony-stimulating factor, IL-8, CCL5/RANTES, CCL20/MIP3A, HLA class I, and VCAM1 were previously reported to be K13/vFLIP-induced proteins, as *Cox2* and *Cxcr7*/*Rdc1* mRNAs (15, 20, 29). We additionally found considerable induction of other chemokines for attraction of monocyte/macrophages, lymphocytes, neutrophils, dendritic cells, and activated T and NK cells; of other proinflammatory cytokines, including *IL-1*α and *IL-1*β; and of other growth factors, including *G-csf* and *Lif* (Table 1). Consistent with K13/vFLIP promoting a proinflammatory, proadhesive, and chemotactic phenotype, we found that K13/vFLIP significantly enhances the attachment of monocytic cells to endothelial monolayers (Fig. 5), and immunohistochemistry of a typical KS lesion confirmed prominent infiltration with $CD68^+$ monocytic cells (Fig. 6). Thus, our results confirmed that K13/vFLIP is a driving force for the recruitment of the inflammatory cell infiltrate that contributes to KS progression (32).

Activation of the NF-κB pathway is an essential component of the pathogenicity of gammaherpesviruses. K13/vFLIP physically associates with IKKγ, and this interaction activates the canonical NF-κB pathway (25). Consistent with its ability to activate the canonical NF-κB pathway, we found that K13/vFLIP stimulates expression of many genes for chemokines, cytokines, growth factors, and surface receptors known to be targets of NF-κB. A chemical inhibitor of NF-κB reduced expression of selected genes induced by K13/vFLIP, and endothelial cells transduced with a mutant K13/vFLIP (K13/$vFLIP^{A57L}$) that no longer binds to IKKγ failed to exhibit increased expression of index genes normally induced by wild-type K13/vFLIP. According to a previous report, K13/vFLIP can also activate the noncanonical NF-κB pathway by physically binding NF-κB2/p100 (27), but the importance of this pathway could not be confirmed in the present study.

K13/vFLIP activated the stress-activated protein kinases p38 and JNK/SAPK in endothelial cells, but not ERK1/2 (Fig. 5A). A potential mechanism for JNK/SAPK activation is through a physical interaction of K13/vFLIP with TRAFs receptor-associated factors) (10, 17), similar to the well-described pathway

initiated by TNF receptor (TNFR) engagement. Another possibility is that these kinases are simply activated as a result of autocrine signaling by inflammatory cytokines such as IL-1β, which is markedly induced by K13/vFLIP in endothelial cells. Regardless of the mechanism for its activation, we found that the p38 kinase is clearly upstream of *Cox2*, since the p38MAPK inhibitor SB202190 selectively reduced expression of COX2.

Erythrocyte-replete vascular slits, edema, and neovascularization are characteristic features of KS histology, which give the lesions a red or purple color. The vascular slits are believed to reflect rudimentary attempts at forming vascular structures by the virally infected cells, likely of endothelial cell lineage. We show that K13/vFLIP disrupts the ability of endothelial cells to form ECM-dependent vascular structures and may thus contribute to formation of a discontinuous vascular system, leading to KS vascular slits. Many factors likely contribute to this defect, but K13/vFLIP stimulates secretion of IP-10, which alone can disrupt ECM-dependent cord formation (2). K13/vFLIP can also enhance expression of SEMA3C and CXCR7/RDC1. Semaphorins are guidance molecules critical to neuronal and vascular development (40). CXCR7/RDC1, a coreceptor for CXCL12/SDF-1, forms heterodimers with CXCR4, a chemokine receptor with essential functions in vascular development and angiogenesis (26, 37, 41). Cox2, through prostaglandin E_2, may provide proangiogenic activity to KS lesions (5).

A most interesting observation we made is that endothelial cells expressing K13/vFLIP are significantly more sensitive to treatment with 5-dFUrd compared to control endothelial cells and are 10 to 100 times more sensitive to 5-dFUrd than cancer cell lines (3, 43). This increased drug sensitivity of endothelial cells is attributable to K13/vFLIP inducing endothelial cell expression of PD-ECGF/TP, an enzyme that converts 5-dFUrd into the active pyrimidine nucleoside 5-FU, which interferes with DNA and RNA synthesis and generate anticancer activity (3, 7). A chemical inhibitor of PD-ECGF/TP specifically reduced 5-dFUrd cytotoxicity for K13/vFLIP-HUVEC, indicating the involvement of PD-ECGF/TP enzymatic activity. 5-dFUrd is an oral drug that has already been tested in several clinical cancer trials (13) and would be a promising compound for the treatment of KS that could be readily tested in KS patients.

ACKNOWLEDGMENTS

This study was supported by the intramural research program of the National Institute of Health, National Cancer Institute, Center for Cancer Research.

We thank Robert Yarchoan, Kathryn Wyvill, and Karen Alteman (CCR, NCI, NIH) for providing KS specimens; G. Nolan (Stanford University, Stanford, CA) for the retroviral vector; Jan Balzarini (Rega Institute for Medical Research, Rega, Belgium) for the KIN59; Susan Garfield and Poonam Mannan (Laboratory of Experimental Carcinogenesis, CCR, NCI, NIH) for the laser confocal microscopy; the Laboratory of Human Carcinogenesis (CCR, NCI, NIH) for providing ABI7900HT; and Lucy Sierra, Paola Gasperini, and Ombretta Salvucci for their help on various aspects of this work.

REFERENCES

1. **An, J., Y. Sun, R. Sun, and M. B. Rettig.** 2003. Kaposi's sarcoma-associated herpesvirus encoded vFLIP induces cellular IL-6 expression: the role of the NF-κB and JNK/AP1 pathways. Oncogene **22:**3371–3385.
2. **Angiolillo, A. L., C. Sgadari, D. D. Taub, F. Liao, J. M. Farber, S. Maheshwari, H. K. Kleinman, G. H. Reaman, and G. Tosato.** 1995. Human interferon-inducible protein 10 is a potent inhibitor of angiogenesis in vivo. J. Exp. Med. **182:**155–162.
3. **Armstrong, R. D., and R. B. Diasio.** 1980. Metabolism and biological activity of 5′-deoxy-5-fluorouridine, a novel fluoropyrimidine. Cancer Res. **40:**3333–3338.
4. **Bagneris, C., A. V. Ageichik, N. Cronin, B. Wallace, M. Collins, C. Boshoff, G. Waksman, and T. Barrett.** 2008. Crystal structure of a vFlip-IKKγ complex: insights into viral activation of the IKK signalosome. Mol. Cell **30:**620–631.
5. **Ben-Av, P., L. J. Crofford, R. L. Wilder, and T. Hla.** 1995. Induction of vascular endothelial growth factor expression in synovial fibroblasts by prostaglandin E and interleukin-1: a potential mechanism for inflammatory angiogenesis. FEBS Lett. **372:**83–87.
6. **Birnie, G. D., H. Kroeger, and C. Heidelberger.** 1963. Studies of fluorinated pyrimidines. XVIII. The degradation of 5-fluoro-2′-deoxyuridine and related compounds by nucleoside phosphorylase. Biochemistry **2:**566–572.
7. **Bose, R., and E. W. Yamada.** 1974. Uridine phosphorylase, molecular properties and mechanism of catalysis. Biochemistry **13:**2051–2056.
8. **Boshoff, C., and R. Weiss.** 2002. AIDS-related malignancies. Nat. Rev. Cancer **2:**373–382.
9. **Burns, J. M., B. C. Summers, Y. Wang, A. Melikian, R. Berahovich, Z. Miao, M. E. Penfold, M. J. Sunshine, D. R. Littman, C. J. Kuo, K. Wei, B. E. McMaster, K. Wright, M. C. Howard, and T. J. Schall.** 2006. A novel chemokine receptor for SDF-1 and I-TAC involved in cell survival, cell adhesion, and tumor development. J. Exp. Med. **203:**2201–2213.
10. **Chaudhary, P. M., A. Jasmin, M. T. Eby, and L. Hood.** 1999. Modulation of the NF-κB pathway by virally encoded death effector domains-containing proteins. Oncogene **18:**5738–5746.
11. **Chugh, P., H. Matta, S. Schamus, S. Zachariah, A. Kumar, J. A. Richardson, A. L. Smith, and P. M. Chaudhary.** 2005. Constitutive NF-κB activation, normal Fas-induced apoptosis, and increased incidence of lymphoma in human herpesvirus 8 K13 transgenic mice. Proc. Natl. Acad. Sci. USA **102:**12885–12890.
12. **Davis, R. J.** 2000. Signal transduction by the JNK group of MAP kinases. Cell **103:**239–252.
13. **Fossa, S. D., A. Flokkmann, M. Heier, M. Aas, B. Moe, R. Heintz, and S. Linder-Ciccolunghi.** 1986. Phase I/II tolerability/pharmacokinetic study with one-hour intravenous infusion of doxifluridine (5′-dFUrd) 3 g/m2 VS 5 g/m^2 QD × 5 per month. Cancer Chemother. Pharmacol. **18:**252–256.
14. **Gifford, C. A., A. M. Assiri, M. C. Satterfield, T. E. Spencer, and T. L. Ott.** 2008. Receptor transporter protein 4 (RTP4) in endometrium, ovary, and peripheral blood leukocytes of pregnant and cyclic ewes. Biol. Reprod. **79:**518–524.
15. **Grossmann, C., S. Podgrabinska, M. Skobe, and D. Ganem.** 2006. Activation of NF-κB by the latent vFLIP gene of Kaposi's sarcoma-associated herpesvirus is required for the spindle shape of virus-infected endothelial cells and contributes to their proinflammatory phenotype. J. Virol. **80:**7179–7185.
16. **Guasparri, I., S. A. Keller, and E. Cesarman.** 2004. KSHV vFLIP is essential for the survival of infected lymphoma cells. J. Exp. Med. **199:**993–1003.
17. **Guasparri, I., H. Wu, and E. Cesarman.** 2006. The KSHV oncoprotein vFLIP contains a TRAF-interacting motif and requires TRAF2 and TRAF3 for signalling. EMBO Rep. **7:**114–119.
18. **Heyes, M. P., K. Saito, E. O. Major, S. Milstien, S. P. Markey, and J. H. Vickers.** 1993. A mechanism of quinolinic acid formation by brain in inflammatory neurological disease. Attenuation of synthesis from L-tryptophan by 6-chlorotryptophan and 4-chloro-3-hydroxyanthranilate. Brain **116**(Pt. 6)**:** 1425–1450.
19. **Hong, Y. K., K. Foreman, J. W. Shin, S. Hirakawa, C. L. Curry, D. R. Sage, T. Libermann, B. J. Dezube, J. D. Fingeroth, and M. Detmar.** 2004. Lymphatic reprogramming of blood vascular endothelium by Kaposi sarcoma-associated herpesvirus. Nat. Genet. **36:**683–685.
20. **Lagos, D., M. W. Trotter, R. J. Vart, H. W. Wang, N. C. Matthews, A. Hansen, O. Flore, F. Gotch, and C. Boshoff.** 2007. Kaposi sarcoma herpesvirus-encoded vFLIP and vIRF1 regulate antigen presentation in lymphatic endothelial cells. Blood **109:**1550–1558.
21. **Lee, E. G., D. L. Boone, S. Chai, S. L. Libby, M. Chien, J. P. Lodolce, and A. Ma.** 2000. Failure to regulate TNF-induced NF-κB and cell death responses in A20-deficient mice. Science **289:**2350–2354.
22. **Ley, K.** 2002. Integration of inflammatory signals by rolling neutrophils. Immunol. Rev. **186:**8–18.
23. **Liekens, S., A. Bronckaers, A. I. Hernandez, E. M. Priego, E. Casanova, M. J. Camarasa, M. J. Perez-Perez, and J. Balzarini.** 2006. 5′-O-tritylated nucleoside derivatives: inhibition of thymidine phosphorylase and angiogenesis. Mol. Pharmacol. **70:**501–509.
24. **Liekens, S., A. I. Hernandez, D. Ribatti, E. De Clercq, M. J. Camarasa, M. J. Perez-Perez, and J. Balzarini.** 2004. The nucleoside derivative 5′-*O*-trityl-inosine (KIN59) suppresses thymidine phosphorylase-triggered angiogenesis via a noncompetitive mechanism of action. J. Biol. Chem. **279:**29598–29605.
25. **Liu, L., M. T. Eby, N. Rathore, S. K. Sinha, A. Kumar, and P. M. Chaudhary.** 2002. The human herpesvirus 8-encoded viral FLICE inhibitory protein physically associates with and persistently activates the IκB kinase complex. J. Biol. Chem. **277:**13745–13751.
26. **Ma, Q., D. Jones, P. R. Borghesani, R. A. Segal, T. Nagasawa, T. Kishimoto, R. T. Bronson, and T. A. Springer.** 1998. Impaired B-lymphopoiesis, myelo-

poiesis, and derailed cerebellar neuron migration in CXCR4- and SDF-1-deficient mice. Proc. Natl. Acad. Sci. USA **95:**9448–9453.
27. **Matta, H., and P. M. Chaudhary.** 2004. Activation of alternative NF-κB pathway by human herpesvirus 8-encoded Fas-associated death domain-like IL-1 beta-converting enzyme inhibitory protein (vFLIP). Proc. Natl. Acad. Sci. USA **101:**9399–9404.
28. **Matta, H., L. Mazzacurati, S. Schamus, T. Yang, Q. Sun, and P. M. Chaudhary.** 2007. KSHV oncoprotein K13 bypasses TRAFs and directly interacts with the IκB kinase complex to selectively activate NF-κB without JNK activation. J. Biol. Chem. **282:**24858–24865.
29. **Matta, H., R. M. Surabhi, J. Zhao, V. Punj, Q. Sun, S. Schamus, L. Mazzacurati, and P. M. Chaudhary.** 2007. Induction of spindle cell morphology in human vascular endothelial cells by human herpesvirus 8-encoded viral FLICE inhibitory protein K13. Oncogene **26:**1656–1660.
30. **Moore, P. S., and Y. Chan.** 2001. Kaposi's sarcoma-associated herpesvirus, p. 2803–2833. *In* D. M. Knipe and P. M. Howley (ed.), Fields virology, 4th ed. Lippincott-Raven Publishers, Philadelphia, PA.
31. **Murga, M., O. Fernandez-Capetillo, and G. Tosato.** 2005. Neuropilin-1 regulates attachment in human endothelial cells independently of vascular endothelial growth factor receptor-2. Blood **105:**1992–1999.
32. **Nakamura, S., S. Z. Salahuddin, P. Biberfeld, B. Ensoli, P. D. Markham, F. Wong-Staal, and R. C. Gallo.** 1988. Kaposi's sarcoma cells: long-term culture with growth factor from retrovirus-infected $CD4^+$ T cells. Science **242:**426–430.
33. **Narazaki, M., and G. Tosato.** 2006. Ligand-induced internalization selects use of common receptor neuropilin-1 by VEGF165 and semaphorin3A. Blood **107:**3892–3901.
34. **Nishino, I., A. Spinazzola, and M. Hirano.** 1999. Thymidine phosphorylase gene mutations in MNGIE, a human mitochondrial disorder. Science **283:**689–692.
35. **Pierce, J. W., R. Schoenleber, G. Jesmok, J. Best, S. A. Moore, T. Collins, and M. E. Gerritsen.** 1997. Novel inhibitors of cytokine-induced IκBα phosphorylation and endothelial cell adhesion molecule expression show anti-inflammatory effects in vivo. J. Biol. Chem. **272:**21096–21103.
36. **Salcedo, R., J. H. Resau, D. Halverson, E. A. Hudson, M. Dambach, D. Powell, K. Wasserman, and J. J. Oppenheim.** 2000. Differential expression and responsiveness of chemokine receptors (CXCR1-3) by human microvascular endothelial cells and umbilical vein endothelial cells. FASEB J. **14:**2055–2064.
37. **Salvucci, O., L. Yao, S. Villalba, A. Sajewicz, S. Pittaluga, and G. Tosato.** 2002. Regulation of endothelial cell branching morphogenesis by endogenous chemokine stromal-derived factor-1. Blood **99:**2703–2711.
38. **Samaniego, F., P. D. Markham, R. Gendelman, Y. Watanabe, V. Kao, K. Kowalski, J. A. Sonnabend, A. Pintus, R. C. Gallo, and B. Ensoli.** 1998. Vascular endothelial growth factor and basic fibroblast growth factor present in Kaposi's sarcoma (KS) are induced by inflammatory cytokines and synergize to promote vascular permeability and KS lesion development. Am. J. Pathol. **152:**1433–1443.
39. **Sarid, R., T. Ben-Moshe, G. Kazimirsky, S. Weisberg, E. Appel, D. Kobiler, S. Lustig, and C. Brodie.** 2001. vFLIP protects PC-12 cells from apoptosis induced by Sindbis virus: implications for the role of TNF-α. Cell Death Differ. **8:**1224–1231.
40. **Serini, G., D. Valdembri, S. Zanivan, G. Morterra, C. Burkhardt, F. Caccavari, L. Zammataro, L. Primo, L. Tamagnone, M. Logan, M. Tessier-Lavigne, M. Taniguchi, A. W. Puschel, and F. Bussolino.** 2003. Class 3 semaphorins control vascular morphogenesis by inhibiting integrin function. Nature **424:**391–397.
41. **Sierro, F., C. Biben, L. Martinez-Munoz, M. Mellado, R. M. Ransohoff, M. Li, B. Woehl, H. Leung, J. Groom, M. Batten, R. P. Harvey, A. C. Martinez, C. R. Mackay, and F. Mackay.** 2007. Disrupted cardiac development but normal hematopoiesis in mice deficient in the second CXCL12/SDF-1 receptor, CXCR7. Proc. Natl. Acad. Sci. USA **104:**14759–14764.
42. **Sun, Q., S. Zachariah, and P. M. Chaudhary.** 2003. The human herpesvirus 8-encoded viral FLICE-inhibitory protein induces cellular transformation via NF-κB activation. J. Biol. Chem. **278:**52437–52445.
43. **Tevaearai, H. T., P. L. Laurent, L. Suardet, J. F. Eliason, J. C. Givel, and N. Odartchenko.** 1992. Interactions of interferon-alpha 2a with 5′-deoxy-5-fluorouridine in colorectal cancer cells in vitro. Eur. J. Cancer **28:**368–372.
44. **Viemann, D., M. Goebeler, S. Schmid, K. Klimmek, C. Sorg, S. Ludwig, and J. Roth.** 2004. Transcriptional profiling of IKK2/NF-κB- and p38 MAP kinase-dependent gene expression in TNF-alpha-stimulated primary human endothelial cells. Blood **103:**3365–3373.
45. **Viemann, D., M. Goebeler, S. Schmid, U. Nordhues, K. Klimmek, C. Sorg, and J. Roth.** 2006. TNF induces distinct gene expression programs in microvascular and macrovascular human endothelial cells. J. Leukoc. Biol. **80:**174–185.
46. **Wang, C. Y., M. W. Mayo, R. G. Korneluk, D. V. Goeddel, and A. S. Baldwin, Jr.** 1998. NF-κB antiapoptosis: induction of TRAF1 and TRAF2 and c-IAP1 and c-IAP2 to suppress caspase-8 activation. Science **281:**1680–1683.
47. **Williams, M. R., N. Kataoka, Y. Sakurai, C. M. Powers, S. G. Eskin, and L. V. McIntire.** 2008. Gene expression of endothelial cells due to interleukin-1 beta stimulation and neutrophil transmigration. Endothelium **15:**73–165.
48. **Wullaert, A., L. Verstrepen, S. Van Huffel, M. Adib-Conquy, S. Cornelis, M. Kreike, M. Haegman, K. El Bakkouri, M. Sanders, K. Verhelst, I. Carpentier, J. M. Cavaillon, K. Heyninck, and R. Beyaert.** 2007. LIND/ABIN-3 is a novel lipopolysaccharide-inducible inhibitor of NF-κB activation. J. Biol. Chem. **282:**81–90.
49. **Yarilina, A., K. H. Park-Min, T. Antoniv, X. Hu, and L. B. Ivashkiv.** 2008. TNF activates an IRF1-dependent autocrine loop leading to sustained expression of chemokines and STAT1-dependent type I interferon-response genes. Nat. Immunol. **9:**378–387.